Topological classification and diagnosis in magnetically ordered electronic materials

Bingrui Peng,[1,2,*] Yi Jiang,[1,2,*] Zhong Fang,[1] Hongming Weng,[1,3] and Chen Fang[1,3,4,†]

[1]*Beijing National Laboratory for Condensed Matter Physics and Institute of Physics, Chinese Academy of Sciences, Beijing 100190, China*

[2]*University of Chinese Academy of Sciences, Beijing 100049, China*

[3]*Songshan Lake Materials Laboratory, Dongguan, Guangdong 523808, China*

[4]*Kavli Institute for Theoretical Sciences, Chinese Academy of Sciences, Beijing 100190, China*

(Received 5 April 2021; revised 18 April 2022; accepted 19 May 2022; published 27 June 2022)

We show that lattice symmetry groups without time reversal, also known as magnetic space group symmetries, protect topological invariants as well as surface states that are distinct from those of nonmagnetic topological states. We obtain, by explicit and exhaustive construction of topological crystals using lower-dimensional building blocks, the full topological classification of electronic band insulators that are magnetically ordered for each one of the 1421 magnetic space groups (MSGs) in three dimensions with significant spin-orbit coupling. Compared with previous works on classification which include the results for some of the MSGs, our unified framework systematically gives the complete classification for all MSGs. We have also computed the symmetry-based indicators (SIs) for each nontrivial class and, by doing so, establish the complete mapping from symmetry representations to topological invariants. Our work goes beyond Elcoro *et al.* [L. Elcoro, B. J. Wieder, Z. Song, Y. Xu, B. Bradlyn, and B. A. Bernevig, Nat. Commun. **12**, 5965 (2021)] by constructing all gapped magnetic topological crystalline states, among which many cannot be diagnosed by SIs. By doing so, we have also identified all SIs that do not correspond to any gapped states but gapless Weyl semimetals.

DOI: 10.1103/PhysRevB.105.235138

I. INTRODUCTION

Magnetic space groups (MSGs) [1] describe the symmetry of lattices where magnetic moments (e.g., spins) are magnetically ordered. Magnetic ordering necessarily breaks time-reversal symmetry (TRS) and, as the order parameter is a vector, usually also breaks some point-group symmetries (rotation and reflection). In many magnetically ordered materials, especially those having antiferromagnetism, there are a special type of composite symmetries: a group element $m = g \cdot T$ is the composition of a space-group (SG) symmetry g and TRS T. Consider, for example, an antiferromagnetic Néel order polarized along z with propagation vector $\mathbf{Q} = (\pi/a, 0, 0)$, where a is the lattice constant. The lattice translation by one unit cell along x, $\{E|100\}$, is broken and time reversal, T, is also broken, while their composition $\{E|100\} \cdot T$ remains a symmetry. [Here we use E to represent the identity 3×3 matrix, representing the trivial element of $O(3)$.] For realistic magnetic materials, their magnetic structure could be more complicated compared to simple collinear configurations, and MSGs are thus required to describe their magnetic orderings. By considering all possible combinations of TRS with SG symmetries, and the absence thereof, there are 1651 Shubnikov SGs (SSGs) which are classified into four types. If there is no antiunitary symmetry, the SSG is type I (i.e., 230 original SGs). The other three types of SSG have the general form of $M = G + m \cdot G$, where m is an antiunitary symmetry. If $m = T$ is the TRS and G is an SG, the SSG is type II; if $m = g \cdot T$, where g is a nontrivial point group operation and G a halving subgroup of an SG, the SSG is type III; and, lastly, if $m = \{E|klm\} \cdot T$, where $\{E|klm\}$ is a pure lattice translation and G an SG, type IV. By this definition, type-II SSGs contain TRS and hence describe nonmagnetic materials. In this paper, we focus on MSGs, i.e., 1421 type-I, -III, and -IV SSGs.

MSGs are also the symmetries of the effective Hamiltonians describing elementary excitations, such as magnons and electrons, that move within a magnetically ordered lattice. In this paper, we focus on magnetic materials in which coherent quasiparticle fermion excitations form band(s) within a finite range of the Fermi energy and study the band topology of these fermions. Our theory can, in principle, be applied to any magnetic materials where the notion of electronlike quasiparticles is valid, at least near the Fermi energy. Itinerant magnets [2], heavy-fermion metals [3], and doped Mott insulators [4] that maintain a magnetically ordered state are considered to belong to this large class of materials.

The interplay between symmetry and topology has been a focus of modern condensed-matter research [5–8]. For a given symmetry group and a nonzero gap, all band Hamiltonians are grouped into *equivalence classes*, where two Hamiltonians in the same (different) class(es) can(not) be smoothly deformed into each other, while maintaining both the gap and the symmetry. Each equivalence class is denoted by a unique set of integers called the *topological invariants* [9–16], the forms and types of which only depend on the symmetry group and dimensionality. How many distinct equivalence classes exist for a given symmetry group in a given dimension, and

*These authors contributed equally to this paper.

†cfang@iphy.ac.cn

TABLE I. Comparison of different methods for computing classifications. K-theory-based methods give the complete classification for each MSG, but only part of type-I symmorphic MSGs are computed [51]. The layer construction method adopted in Ref. [52], where only MSGs having nontrivial SIs are treated, cannot guarantee the complete classification for each MSG, as there exist a large number of nonlayer constructions. The *real-space recipe* we use in this paper, however, can obtain complete classifications for all MSGs.

K theory	Classification for type-I symmorphic MSGs
Layer construction	Classification for MSGs with SI
Real-space recipe	Complete classifications for all MSGs with and without SI

what are the topological invariants for each class? This is the question we call the problem of *topological classification*. The theory of topological classification for time-reversal and particle-hole symmetries has been done in all dimensions using the K theory [17–19]; the classification problem for a single spatial symmetry plus time reversal in three dimensions has been solved, usually heuristically, for several symmetries [20–29], and the classification problem for arbitrary SGs plus time reversal in three dimensions has been attempted using either the real-space recipe argument [30–32] or the double-strong-topological-insulator construction [26,33] argument more recently.

The classification problem of magnetic topological crystalline insulators (MTCIs), i.e., gapped topological crystalline states protected by MSGs, begins with the theory of axion insulators protected by space-inversion symmetry without time reversal [6,28,34–42], followed by the theory of antiferromagnetic topological insulators [43–46], again followed by the discovery of several topological invariants protected by wallpaper groups (WGs) [47,48] and magnetic point groups (MPGs) [49,50] as well as part of type-I symmorphic MSGs [51]. A more systematic attempt is made in Ref. [52], where the layer-construction (LC) method reveals a number of unique topological states. In this paper, we use the *real-space recipe* method developed in Refs. [31,32] to complete MTCI classification for all MSGs, which was not achieved by previous schemes, including K-theory [51] and the LC method [52]. A comparison of these methods are shown in Table I. Effectively, the *real-space recipe* converts the problem of topological classification into a LEGO puzzle, where one tries to find distinct ways one can build an edgeless construction using some given pieces. Each piece has a gapless edge state, which should cancel with edge states of adjacent pieces on the common edge they meet to fulfill the condition that the bulk is fully gapped. This LEGO puzzle is then further transformed into finding all independent integer solutions of a set of linear equations on a $\mathbb{Z}_n$ ring. This method not only yields a complete topological classification of gapped bands in each of the 1421 groups, but also gives us, for each nontrivial equivalence class, one explicit and microscopic construction that we call the topological crystal (TC) [31]. We emphasize that our method finds more topological classes than the LC method because LCs are a type of TCs, while not all TCs are LCs. (In fact, we show that at least 553 of the 1421 MSGs have at least one topological state that cannot be layer constructed.)

TABLE II. Summary of preceding works on magnetic topological states. We remark that Ref. [52] used the layer construction method to obtain the interpretations of SIs (but omitted nonlayer constructions), and discussed only part of the gapless SIs. Reference [70] studied several type-IV MSGs with gapless SIs together with other gapless phases that lie out of the scope of SIs.

<table>
<tr><th colspan="2">Topology in MSGs</th><th colspan="3">Previous works</th></tr>
<tr><td colspan="2">Invariant and surface state</td><td colspan="3">P[6, 28, 34–36], $T\cdot\{E|t\}$[43–46], $C_n\cdot T$[24, 53, 63–65], glide[53, 66–69]</td></tr>
<tr><td colspan="2">Classifications</td><td colspan="3">WGs[47, 48], MPGs[50]
Type-I symmorphic MSGs[51]</td></tr>
<tr><td colspan="2">Real-space constructions</td><td colspan="3">Layer constructions of MSGs with SI[52]</td></tr>
<tr><td colspan="2">SI groups</td><td>All MSGs[61]</td><td rowspan="3">Type-I MSGs[60]</td><td rowspan="3">All MSGs[52]</td></tr>
<tr><td colspan="2">SI formulas</td><td>P: [28, 36]</td></tr>
<tr><td rowspan="2">SI interpretations</td><td>Gapped</td><td>C_n: [54]</td></tr>
<tr><td>Gapless</td><td>Type-IV[70]</td><td colspan="2"></td></tr>
</table>

If the classification gives us the labels (topological invariants) for the equivalence classes into which gapped states are put in, the *topological diagnosis* then tells us to which equivalence class a specific, given material (Hamiltonian) belongs. Ideally, a diagnosis scheme computes the topological invariants of that Hamiltonian, and by comparing these values with the labels on the equivalence classes, one puts the Hamiltonian into the right one. However, topological invariants are notoriously difficult to compute [23,53] and, for some, we do not even have the explicit expressions in terms of the wave functions of the bands [25,26]. Fortunately, if we relax the requirement of ideal diagnosis to approximate diagnosis, the story is completely changed. An approximate diagnosis uses partial information on the wave function, and in return gives us partial information on the topological invariants, not invariants themselves. For example, an approximate diagnosis for systems with n-fold rotation symmetry yields the invariant (Chern number) modulo n by using only the rotation eigenvalues at several high-symmetry momenta [28,54]. Recently, the theory of symmetry-based indicators (SIs) [55] and that of topological quantum chemistry [56], enhanced by the full mapping from indicators to topological invariants [30], give birth to a fast approximate diagnosis scheme. This fast-diagnosis scheme has been applied to a large number of nonmagnetic materials [57–59]. SI theory in MSGs has been partly tackled in previous works, with SI formulas for type-I MSGs derived by Ono and Watanabe [60] and SI group structures in all SSGs provided by Watanabe *et al.* [61]. More recently, Elcoro *et al.* [52] gave all SI formulas in SSGs and used the LC method to obtain the physical interpretations for SIs that are LC representable. Several hundreds of magnetic topological materials have also been predicted using SIs [62]. We summarize the preceding works on classification and diagnosis of magnetic topological states in Table II.

In this paper, we rederive the explicit formulas for all SIs in terms of band representations (which in part differ from previous works [52,60]) and we calculate the values of SIs

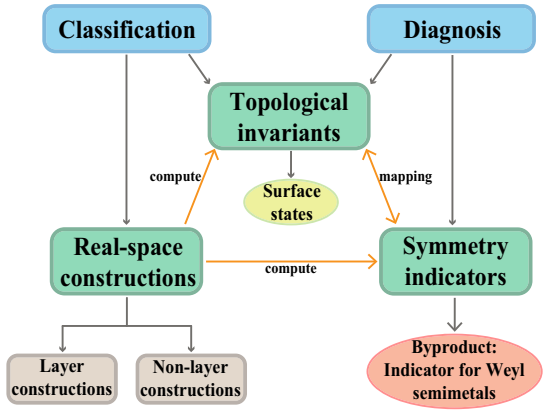

FIG. 1. The main content of this paper, including the classification and diagnosis of gapped topological states in MSGs. The real-space recipe is adopted to construct topological crystals to obtain the classifications, which turn out to include both layer and nonlayer constructions. We exhaust all topological invariants together with their corresponding surface states and derive explicit formulas for symmetry-based indicators (SIs) in MSGs for the purpose of diagnosis. By computing invariants and SIs for real-space constructions, we found the quantitative mappings between invariants and SIs. As a byproduct, we find all SIs that do not correspond to any gapped states, which thus correspond to Weyl semimetals in MSGs.

for each TC in every MSG. As each gapped state can be adiabatically continued to a TC, this result in fact yields the mapping from invariants to SIs. In this calculation, we find that certain SI values are never taken in any TC, and hence can only indicate nodal band structures [71–88]. This is a major advantage of our work as the classification we obtained exhausts all gapped MTCIs, which allow us to identify SIs for gapless states. These nodes are evasive as they are away from any high-symmetry points (HSPs) or lines. In fact, we show that all these nodal indicators indicate Weyl nodes at generic momenta or pinned to a high-symmetry plane in the Brillouin zone (BZ). In a numerical diagnosis, the indicators are by far easier to obtain than the invariants because the former only depend on the band representations at fewer than or equal to eight momenta and the latter depend on the valence-band wave functions in the entire BZ. Therefore, an inverse mapping from SIs to invariants/nodes is generated using a script, provided along with the paper in Ref. [89]. In Fig. 1, we show the main contents of our work. We refer to many details in our lengthy Supplemental Material [90].

II. CLASSIFICATION

A. General scheme

It has been argued in Refs. [91–93] that symmetry-protected topological states (SPTs) protected jointly by on-site and crystalline symmetries can be constructed by placing SPTs protected by on-site symmetries alone in a symmetric way that maintains crystalline symmetries and under the condition of being fully gapped in the bulk, as well as being stable under adding trivial states. This idea of real-space construction, when applied to noninteracting topological crystalline insulators (TCIs), becomes that all TCIs can be adiabatically deformed into a special form of real-space constructions called topological crystals, which means classifying TCIs is equivalent to classifying TCs. TCs are real-space patterns built from topological pieces in lower dimensions, which were first applied to nonmagnetic SGsto obtain the full classifications of nonmagnetic TCIs [31], with results consistent with those obtained by doubled-strong-topological-insulator method [33]. In nonmagnetic SGs, the lower-dimensional pieces are 2D topological insulators and mirror Chern insulators, protected by on-site symmetry TRS and possible mirror symmetry, and have gapless edge states. They are arranged by SG symmetries in real space in a symmetric way such that all edge states cancel with each other, resulting in a fully gapped bulk. This scheme has also been applied to interacting bosonic systems to obtain the SPT classifications, where the whole symmetry groups are direct products of on-site symmetries and spatial symmetries [32,94–96]. The physical validity of the real-space construction can be argued, as in Ref. [92], as follows. By adding a fine mesh of trivial degrees of freedom, the correlation length can be made as small as desired, which allows the reduction of general crystalline SPT states to TCs built from well-defined lower-dimensional states. In this paper, we apply the real-space recipe to construct TCs to obtain the complete classification of all gapped topological states protected by MSGs.

To start, we build a structure of a cell complex by using MSG symmetries, including both unitary and antiunitary ones, and partition the 3D space into finite 3D regions called asymmetric units (AUs) that fill the whole 3D space without overlaps. In fact, all AUs are symmetry related and can be generated by choosing one AU and then copying it using MSG operations. AUs are also called 3-cells, and the 2D faces where they meet are 2-cells. Similarly, 1D lines where 2-cells intersect are 1-cells, and the endpoints of 1-cells are 0-cells. The interior of an AU consists of generic Wyckoff positions which have only the identity symmetry, while high-symmetry Wyckoff positions always lie on the boundary of AUs, i.e., 2-, 1-, and 0-cells.

To construct TCs in 3D, we should take account of all d-dimensional topological building blocks with $d \leqslant 3$. For each cell, its local symmetry group is defined as the collection of symmetries that keep every point of the cell unchanged. The local symmetry group of a cell determines the on-site symmetry class (Altland-Zirnbauer class [97]) of the Hamiltonian on that cell. For MSGs, the effective symmetry class of a cell is always class A or class AI. Note that although some cells have a mirror plane as on-site symmetry, the states on them can be divided into two sectors by mirror eigenvalues, each of which belongs to class A. A 2-cell may have a local symmetry group generated by $M \cdot T$, and a 1-cell local symmetry group generated by $C_2 \cdot T$. Because $(M \cdot T)^2 = (C_2 \cdot T)^2 = +1$, those cells belong to symmetry class AI. According to the tenfold way results [19], systems of class AI have trivial classification in 1D, 2D, and 3D, and nontrivial classification in 0D, while systems of class A have nontrivial classification in 0D and 2D and trivial classification in 1D and 3D. As shown in Ref. [31], 0D states can be considered as trivial atomic insulators [98], which means only 2D topological building blocks need to be considered in the construction of TCs for MSG. Furthermore,

there are two types of 2-cells depending on whether they coincide with mirror planes. If they coincide, they can be decorated with mirror Chern insulators characterized by two $\mathbb{Z}$ numbers, i.e., two mirror Chern numbers for $\pm i$ mirror sectors and, if not, with Chern insulators characterized by one $\mathbb{Z}$ number, i.e., the Chern number. Therefore, there are only two types of building blocks for our real-space recipe, i.e., Chern insulators and mirror Chern insulators. We remark that due to the absence of TRS in MSGs, the mirror Chern insulator we use here does not require two mirror Chern numbers to be opposite with each other, i.e., $C_m^+ \neq C_m^-$ generically, which are different from the mirror Chern insulators in nonmagnetic SGs with $C_m^+ = -C_m^-$ [21,22].

Having building blocks in hand, we next enumerate all topological inequivalent decorations on the cell complexes in MSGs. Before proceeding, note that the building blocks themselves form a finitely generated Abelian group, e.g., $\mathbb{Z}$ for Chern insulators and $\mathbb{Z}^2$ for mirror Chern insulators. Therefore, the TCs built from them form a linear space with integer coefficients, such that two TCs can be added to obtain another TC, and there exists a maximal set of linearly independent TCs (the generators) for each MSG. As a result, one just needs to obtain the generators to describe the full set of TCs. As TCs are supposed to be fully gapped topological states, all the boundary states contributed by 2D building blocks (Chern insulators and mirror Chern insulators) should cancel with each other on each 1-cell, leading to fully gapped states inside the bulk, a condition known as the gluing condition [31] or no-open-edge condition [32]. After this procedure, we obtain a set of generators that form an Abelian group $\mathbb{Z}^n$. However, this is generally not the final classification because some generators will reduce from $\mathbb{Z}$ type to $\mathbb{Z}_2$ type after a process of subtracting topological trivial elements called bubble equivalence [31,32]. The final classification can be expressed as a quotient group Ker/Img, a structure resembling group (co)homology, where Ker stands for the linear space of TCs satisfying no-open-edge condition and Img for the space of bubble-equivalence. These final classifications of MSGs have the form $\mathbb{Z}^n \times \mathbb{Z}_2^l$ and can be found in Supplemental Material [90] Sec. O.

In Fig. 2, we show the procedures for constructing TCs in MSG $P4$. Figure 2(a) shows the cell complex of $P4$, where the unit cell is partitioned into four cuboids (i.e., four AUs) by the C_4 symmetry, and three colored facets denote three independent 2-cells. As there is no mirror symmetry in $P4$, the only building block is the 2D Chern insulator. In Fig. 2(b), we plotted the TC generated by placing a Chern insulator with $C = 1$ on the green 2-cell. Because C_4 and translation symmetry preserve the direction of chiral edge states of the green 2-cell, the generated TC consists of complete 2D Chern insulator layers on $z \in \mathbb{Z}$ planes, which is a 3D quantum anomalous Hall (QAH) state. In Figs. 2(c) and 2(d), Chern insulators are placed on the red and yellow 2-cells. However, in (c) and (d) (or any linear combinations of them), there exist 1-cells (e.g., vertical green lines) where symmetry-related 2-cells meet, having chiral edges states that run in the same direction and fail to cancel each other, which means their bulk states are gapless. As a result, the only possible TC in $P4$ is (b), which is characterized by the weak invariant (Chern number) and leads to the $\mathbb{Z}$ classification of this MSG.

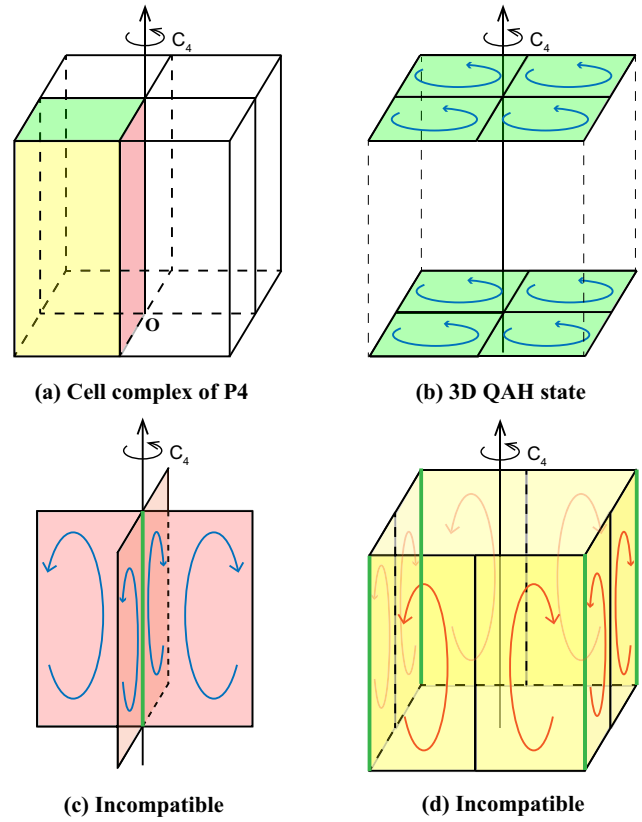

FIG. 2. Procedures for constructing topological crystals. (a) The cell complex of MSG $P4$, where the unit cell is partitioned by C_4 into four AUs, and the three colored facets denote three independent 2-cells. (b) Placing Chern insulators on the green 2-cells generates a 3D quantum anomalous Hall state. (c), (d) Placing Chern insulators on the red or yellow 2-cells cannot generate compatible TCs, as their edge states fail to cancel each other, e.g, on the vertical green 1-cells.

Lastly, we compare the real-space constructions for nonmagnetic SGs and MSGs. First, observe that their building blocks are different. In nonmagnetic SGs, due to the TRS, the building blocks are two-dimensional topological insulators and mirror Chern insulators with $C_m^+ = -C_m^-$, while in MSGs, the building blocks are Chern insulators and mirror Chern insulators with independent C_m^+ and C_m^-. More significantly, for nonmagnetic SGs, one can obtain most of the TCs by LCs, which involve only layered 2D TIs and mirror Chern insulators as building blocks [30], with only 12 nonmagnetic SGs having states beyond LCs [31]. However, non-LCs exist widely in MSGs, and constructing with layers only may lose a number of TCs. By contrast, the real-space recipe employing the structure of the cell complex automatically includes both LCs and non-LCs, giving the complete collection of TCs, hence the complete classification of gapped topological states.

B. Topological invariants

MTCIs are characterized by crystalline-symmetry-protected topological invariants. Previous works have looked into some of the topological invariants protected by magnetic crystalline symmetries, with the earliest one being the axion insulators with inversion invariants [28,36], followed by

TABLE III. MSG symmetries and their corresponding invariant types. We use the Seitz symbol $\{O|t\}$ to represent symmetries with nonzero translations, where R denotes a lattice translation and t a fractional translation. The invariants of the unitary screw and antiunitary glide are bound to the translation invariant, with their values being $\frac{1}{n}$ and $\frac{1}{2}$ of the translation invariant, respectively. All $\mathbb{Z}$ invariants correspond to either the Chern number or mirror Chern number and all $\mathbb{Z}_2$ invariants correspond to the axion angle θ (when all $\mathbb{Z}$ invariants are zero).

MSG symmetries	Invariant type and interpretation
Unitary rotation C_n, Antiunitary improper point group Symmetries $P\cdot T$, $M\cdot T$, $S_n\cdot T$	Trivial
Unitary improper S_n, P, $\{M\|\frac{1}{2}\}$ Antiunitary translation $\{E\|t\}\cdot T$ Antiunitary proper $C_n\cdot T$, $\{C_n\|t\}\cdot T$	$\mathbb{Z}_2$: Axion angle
Unitary translation $\{E\|R\}$ Unitary mirror M Unitary screw $\{C_n\|t\}$ Antiunitary glide $\{M\|\frac{1}{2}\}\cdot T$	$\mathbb{Z}$: (mirror) Chern number

the antiferromagnetic topological insulators protected by antiunitary translations [43,44]. In this paper, we exhaustively enumerate all topological invariants in MSGs.

Formally, having nontrivial symmetry-protected topological invariants means a topological state cannot be smoothly deformed into a trivial state when the symmetry is preserved. Especially, if a MTCI cannot be adiabatically connected to an atomic insulator with the symmetry operation g preserved, we say it has a nontrivial g invariant. As all MTCIs are adiabatically connected to TCs, we can utilize TCs to derive all invariants protected by MSG symmetries. In our real-space recipe, given a symmetry operation g alone, if nontrivial TCs compatible with g can be constructed, then we say g can protect nontrivial topological invariants. More specifically, each independent TC corresponds to an independent invariant, and they have the same group structure, e.g., a $\mathbb{Z}_2$ TC owns a $\mathbb{Z}_2$ invariant.

To find which symmetry operations in MSGs can protect nontrivial invariants and what kinds of the invariants they protect, we take account of all of MSG symmetries one by one, including translation, rotation, inversion, mirror, rotoinversion (S_n), screw, glide, and those combined with TRS such as $C_n\cdot T$, etc. We consider when each of them is present alone, what TCs can be constructed. If no TC exists, this symmetry has only a trivial invariant; if TCs exist, this symmetry must protect nontrivial topological invariants, and we further decide how many independent TCs and whether they are $\mathbb{Z}$ type or $\mathbb{Z}_n$ type by checking if the TCs can be smoothly deformed into trivial states after multiplying n times. In this way, we know all the MSG symmetries that can singly protect nontrivial topological invariants, with each symmetry hosting at most one invariant, being either $\mathbb{Z}_2$ type or $\mathbb{Z}$ type. We summarize the results in Table III and classify these invariants into three types:

(1) Trivial invariants: C_n rotations and antiunitary improper point group symmetries in MSGs cannot host nontrivial decorations. Take C_2, for example. When there is only a C_2 symmetry alone, consider a 2D plane that passes the C_2 axis, which is partitioned into two 2-cells by the axis. Chern insulators cannot be decorated on the two 2-cells, because their chiral edge modes on the C_2 axis are C_2 related, and as such are in the same direction and cannot gap out each other. This is different from the nonmagnetic case where C_2 has a $\mathbb{Z}_2$ invariant [30,31], as the building blocks in nonmagnetic SGs are 2D TIs and two C_2-related helical edge states can cancel with each other.

(2) $\mathbb{Z}$ invariants: Unlike nonmagnetic MSGs where only mirror symmetries have $\mathbb{Z}$ invariants (i.e., mirror Chern number), here in MSGs, as the building blocks are both $\mathbb{Z}$ type, we have many other $\mathbb{Z}$ invariants, including the invariant of unitary translation, unitary screw, and antiunitary glide, which are all related to the Chern number.

(3) $\mathbb{Z}_2$ invariants: A large proportion of MSG symmetries protect $\mathbb{Z}_2$ invariants, with many of them unique to MSGs, such as antiunitary translations/rotations/screws. In Supplemental Material [90] Sec. D, we define a special type of decoration called Z_2 decoration, which has zero weak invariants and all $\mathbb{Z}_2$ invariants bond together and equal to 1 (for mirror Chern numbers, we can define $(C_m^+ + C_m^-)$ mod 2 as a $\mathbb{Z}_2$ invariant), and can be seen as an axion insulator with the axion angle $\theta = \pi$. For Z_2 decorations, all these $\mathbb{Z}_2$ invariants merge into one $\mathbb{Z}_2$ invariant, i.e., the axion invariant, whose definition can be taken as the 3D magnetoelectric polarization P_3 according to Refs. [6,34,54]. For decorations with nonzero $\mathbb{Z}$ invariants, $\mathbb{Z}_2$ invariants can still be defined, but are origin-(convention-) dependent and no longer indicate axion insulators [99].

Each nontrivial invariant has its distinct anomalous surface state due to the bulk-boundary correspondence. Because the topological invariants together with their surface states can be superimposed, we only need to derive the surface state for every single invariant, and the surface states of all MTCIs can be readily known from their invariants. Among these surface states in MSGs, some have already been discussed in previous works, including those protected by $C_2\cdot T$ [24,53,63,64], $C_4\cdot T$ [65], glide [53,66–69], and antiunitary translation [43,44,100], etc. (for spinless invariants including $C_n\cdot T$ and antiunitary translation, see Refs. [45,46]), while some are first proposed in this paper, such as the one protected by antiunitary glide. We plot these surface states in Fig. 3, and more details can be found in Supplemental Material [90] Sec. C. As an example shown in Fig. 3(3), on a cylinder geometry, the surface states protected by $C_n\cdot T$, $n = 2, 4, 6$ have a single Dirac cone on the top surface, and n chiral hinge modes related to each other under $C_n\cdot T$ on the side surface.

Although we find all the topological invariants protected by MSG symmetries, we have not derived their explicit formulas in k space, which could be complicated. Instead, we compute these topological invariants in real space for the TCs we built using a unified method as follows [31]. Given an MSG M and an element $g \in M$, first choose a generic point r inside an arbitrary AU, then draw a path connecting r and its image

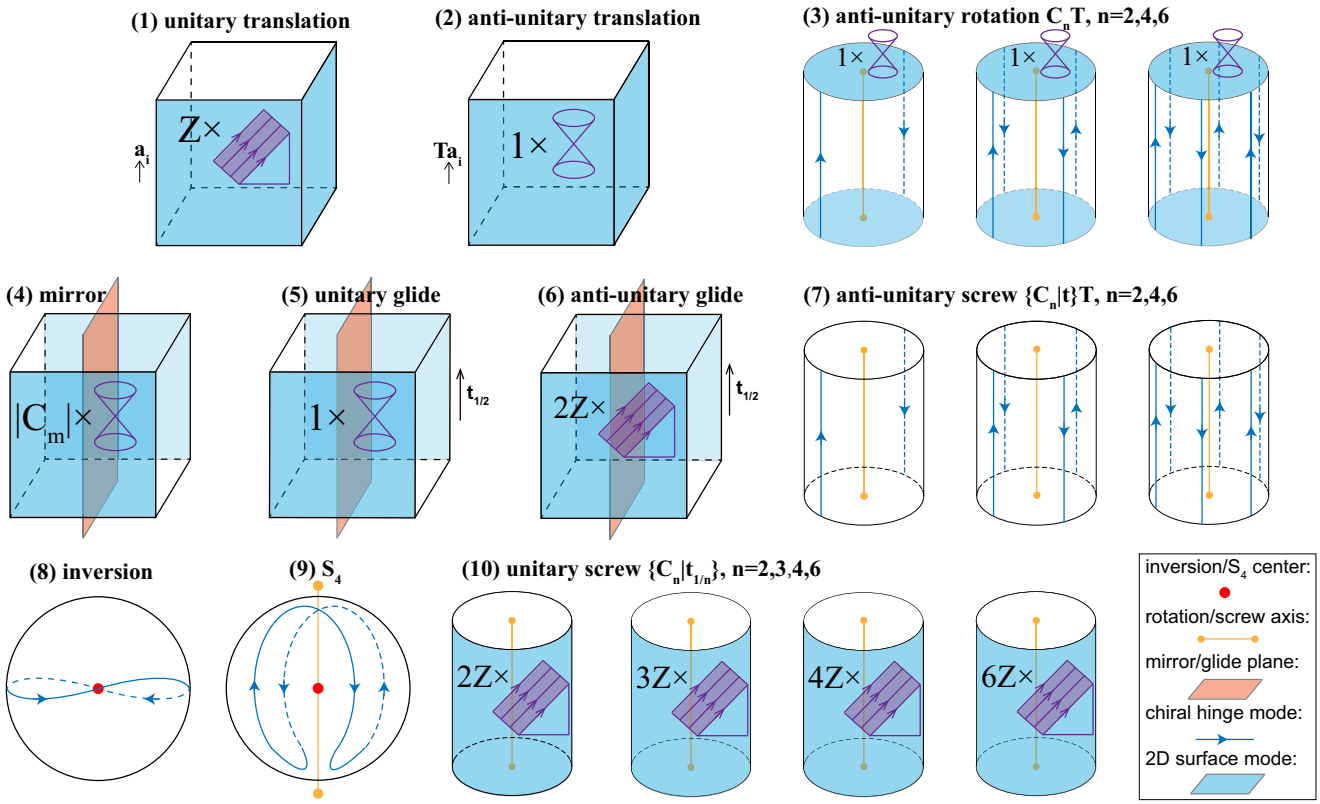

FIG. 3. Surface states of symmetries with nontrivial topological invariants in MSGs, with the surface terminations preserving corresponding symmetries. These surface states can be 1D chiral hinge modes and 2D surface modes, with 2D modes being either slopelike chiral surface modes in (1), (6), (10), or Dirac cones in (2)–(5). More details can be found in Supplemental Material [90] Sec. C.

point $g \cdot r$, under the only constraint that the path does not cross any 1-cells and 0-cells. The corresponding invariant $\delta(g)$ is determined by the decorated 2-cells that the path crosses, i.e., the total Chern number or mirror Chern number accumulated through the path. The invariants thus calculated are well-defined and do not depend on the choice of the generic point r or the path. The full listing of topological invariants of the TCs will prove to be useful in the Sec. III, where we use SIs to diagnose topological states, and TCs function as an intermedium to connect SIs and invariants.

We take one example to show the correspondence between invariants and surface states for a given MSG. The type-III MSG 3.3 $P2'$ has three independent generators of TCs. One of them is protected by $C_{2y} \cdot T$ with nonzero invariant $\delta(C_{2y} \cdot T) = 1$ (i.e., a $C_{2y} \cdot T$-protected axion insulator), while the other two are protected by the translation symmetries in x and z directions, with nonzero weak invariant $\delta(\{E|100\}) = 1$ and $\delta\{E|001\} = 1$, respectively (i.e., 3D QAH states with x/z-directional QAH vectors). For the first decoration, the surface state protected by $C_{2y} \cdot T$ has been described before, as shown in Fig. 3(3), while the other two translation decorations have one chiral surface mode on the 2D surface preserving the translation symmetry in the x/z direction, as shown in Fig. 3(1).

C. Nonlayer constructions

The abundance of non-LCs distinguishes the TCs in MSGs from those in nonmagnetic SGs, where most of the decorations are LCs. In fact, LCs are just a special type of TCs where 2D planes are uniformly decorated, while non-LCs contain nonuniform decorations or incomplete 2D planes.

We use type-I MSG *Pmmm* as a representative to show the characters of non-LCs. *Pmmm* has three orthogonal mirrors M_x, M_y, and M_z, which do not commute with each other due to the spin rotation. Placing mirror Chern insulator layers with $(C_m^+, C_m^-) = (1, -1)$ on any of the six mirror planes, i.e., $x, y, z = 0, \frac{1}{2}$, forms six independent LCs. However, one can still construct a distinct nonlayer decoration falling outside the linear space of these six LCs. As shown in Fig. 4, this nonlayer decoration is constructed by sewing small patches of mirror Chern insulators with $(C_m^+, C_m^-) = (1, 0)$ or $(0, -1)$ on each mirror 2-cell, with adjacent patches having opposite mirror Chern numbers, making each mirror plane nonuniform. Each 1-cell is shared by four patches, with patches in different directions contributing opposite chiral edge modes, canceling with each other and satisfying the no-open-edge condition. Take $z = 0$ plane as an example, where all adjacent 2-cells are related by M_x or M_y. As both Chern number and M_z eigenvalues are reversed under $M_{x,y}$, if one patch has mirror Chern numbers (1,0), then the other two patches adjacent to it must have mirror Chern numbers $(0, -1)$. More detailed discussions for the transformation properties of (mirror) Chern numbers are given in Supplemental Material [90] Sec. A.

This non-LC is distinct from LCs, where each mirror plane is decorated with a uniform, infinite-sized mirror Chern insulator. The decorated 2-cells of this non-LC are all pinned on the mirror planes, preventing it to be deformed into an LC.

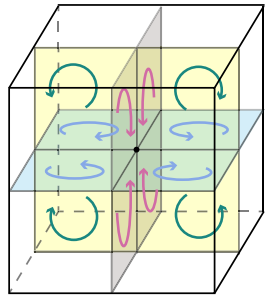

FIG. 4. The non-LC of *Pmmm*, where the arrows denote the directions of the chiral edge modes on the 2-cells. Note we only plot the 2-cells around the origin point inside the unit cell, and omit the six side surfaces for simplicity, which are in fact all decorated. Assume eight inversion centers have coordinate $\boldsymbol{r} = \frac{1}{2}\mathbf{a}_1\delta_1 + \frac{1}{2}\mathbf{a}_2\delta_2 + \frac{1}{2}\mathbf{a}_3\delta_3$, where $\delta_i = 0, 1$ and $\mathbf{a}_i$ is the lattice vector. The 2-cells around an inversion center have the same decoration as shown in the figure if $\sum_i \delta_i$ is even, while the 2-cells have opposite directional edge modes if $\sum_i \delta_i$ is odd.

Although this non-LC seems complicated, we observe that it can be connected to the time-reversal strong TI (STI) from the perspective of surface states. On the one hand, this non-LC has mirror Chern numbers $(C^+_{m,k_i=0}, C^-_{m,k_i=0}, C^+_{m,k_i=\pi}, C^-_{m,k_i=\pi}) = (1, -1, 0, 0)$, $i = x, y, z$, which lead to a nontrivial mirror-protected surface state with a single Dirac cone on $k_i = 0$ in the 2D surface BZ. On the other hand, an STI put on *Pmmm* lattice also has a single Dirac cone on each surface. By the principle of bulk-edge correspondence, we conclude that the STI with *Pmmm* symmetry can be adiabatically deformed into this non-LC by breaking the TRS while preserving crystalline symmetries. Note that for *Pmmm*, despite the absence of TRS, the three mirrors anticommuting with each other also enforce the energy bands to form Kramers-like pairs, i.e., twofold degeneracy with the same parity and opposite mirror eigenvalues. Therefore, the three mirror symmetries still pin the surface Dirac cone on the mirror invariant lines when the TRS is broken. As a result, we can use the tight-binding models of STIs, for example, the 3D Bernevig-Hughes-Zhang (BHZ) model[101], to describe this non-LC.

As mentioned before, unlike nonmagnetic SGs where only 12 SGs have non-LCs [31], non-LCs exist widely in MSGs. For instance, all the supergroups of MSG 47.249 *Pmmm* can host a non-LC as one of its MTCI classification generators, and similar for MSG 25.57 *Pmm*2, 84.51 $P4_2/m$, 10.44 $P2'/m$, 75.3 $P4'$, 6.21 P_am, and 75.5 P_C4, thus the total number of MSGs that have non-LCs is at least 553, i.e., the number of the supergroups of these MSGs, including MSGs with different Bravais lattices. As argued in Ref. [31], STI is compatible with all crystalline symmetries, thus the abundance of non-LCs in MSGs can be understood in a way that they can be obtained by inducing magnetism in STIs in different lattices.

We remark that the non-LCs in these MSGs, when being a Z_2 decoration, are all axion insulators. As STIs are also axion insulators, when the TRS is broken, there still exist other unitary improper or antiunitary proper symmetries that have nontrivial $\mathbb{Z}_2$ invariants, preserving the quantized π axion angle. In the above example of *Pmmm*, the axion angle θ is quantized by $M_{x,y,z}$ and inversion.

TABLE IV. Generating SIs and generating MSGs in MSGs. We use a simplified notation to represent the SI group, i.e., $\mathbb{Z}_{n_1,n_2,\cdots} = \mathbb{Z}_{n_1} \times \mathbb{Z}_{n_2} \times \cdots$. Among these generating MSGs, only $Pnc'c'$ are type-III MSGs, while all the others are type I. The definition and interpretation of these SIs can be found in Supplemental Material [90] Sec. G.

MSG	$\boldsymbol{X}_{\mathrm{BS}}$	SI
$P\bar{1}$	$\mathbb{Z}_{2,2,2,4}$	$z_{2P,1}, z_{2P,2}, z_{2P,3}, z_{4P}$
Pmmm	$\mathbb{Z}_{2,2,2,4}$	$z'_{2P,1}, z'_{2P,2}, z'_{2P,3}, z'_{4P}$
Pn, $n = 2, 3, 4, 6$	$\mathbb{Z}_n$	z_{nC}
Pn/m, $n = 2, 3, 4, 6$	$\mathbb{Z}_{n,n,n}$	$z^+_{nm,0}, z^-_{nm,0}, z^+_{nm,\pi}$
$P\bar{4}$	$\mathbb{Z}_{2,2,4}$	$z_{2,S_4}, z_{2,\mathrm{Weyl}}, z_{4C}$
$P4/mmm$	$\mathbb{Z}_{2,4,8}$	$z'_{2P,1}, z^+_{4m,\pi}, z_8$
$P6/mmm$	$\mathbb{Z}_{6,12}$	$z^+_{6m,\pi}, z_{12}$
$Pnc'c'$, $n = 2, 4, 6$	$\mathbb{Z}_n$	z'_{nC}

III. DIAGNOSIS

The symmetry-based indicator (SI) is a powerful tool for diagnosing topological states [55,56,102] and has been applied in both nonmagnetic SGs [30,33,103] and MSGs [52,60,61,70], leading to the discovery of a significant number of unique topological materials [57–59,62].

However, the mappings between SIs and topological invariants in MSGs have not been fully investigated. In this paper, we derive the explicit formulas of all SIs, and their quantitative mappings to topological invariants if correspond to gapped states, and possible Weyl point configurations if correspond to gapless states. These two different correspondences are found thanks to the MTCI classifications, which exhaust all gapped MTCI states. Specifically, we compute SI for each TC and, by assuming the classification by real-space construction is complete [91–93], SI values not taken by any TC must correspond to gapless states. We remark that all HSP semimetals and high-symmetry line (HSL) semimetals [57] are not considered in this paper, which have representation-enforced nodes on HSPs or along HSLs that necessarily break the compatibility relations and lie outside the scope of SI theory.

A. Explicit expression of SIs

Among 1421 MSGs, 688 of them have nontrivial SIs. Despite the seemingly large number, SIs in all MSGs can be induced from 16 generating MSGs, which we list in Table IV, with only ten corner cases to be discussed later.

Most of the SIs can be expressed in terms of some topological invariants. In fact, the idea of diagnosing nontrivial topology using only the symmetry data on HSPs in the BZ stems from the Fu-Kane formula [16] for nonmagnetic SGs with inversion symmetry, and in the following works [28,36,54] C_n rotation eigenvalues are used to calculate the Chern number modulo n, i.e., the z_{nC} indicator in Table IV. When there exist mirror planes perpendicular to the rotation axis, the z_{nC} indicator can be applied to two mirror sectors which give the $z^{\pm}_{nm,0/\pi}$ indicator, where $\pm$ represents two

mirror sectors. There are also three type-III generating MSGs $Pnc'c'$, $n = 2, 4, 6$ which have antiunitary glide symmetries that make all irreducible corepresentations (coirreps) twofold degenerate (with the same C_n eigenvalues) on the $k_z = \pi$ plane, allowing the definition of a new set of SIs z'_{nC} using the number of degenerate pairs, the value of which corresponds to the Chern number divided by two modulo n of the 2D BZ. The interpretations of other generating SIs are left in Supplemental Material [90] Sec. G.

The word "generating" means the SIs in other MSGs can be expressed in terms of these generating SIs. Some times, the generation involves the reduction of the SI group, e.g., from $\mathbb{Z}_4$ to $\mathbb{Z}_2$ by taking only the even numbers in $\mathbb{Z}_4$. Moreover, the interpretation of the SI, generated from the same generating SI, can be different in different MSGs. For example, the z_{nC} indicator originally represents the Berry phase of a closed loop in the 2D BZ as shown in Supplemental Material [90] Sec. K, and it becomes the Chern number when the state is gapped. However, as shown later, in some other groups, this indicator, if nonzero, indicates gapless topological states, and its value represents the number of Weyl points. For another example, the z'_{4P} indicator is adopted in some MSGs where the co-irreps are not doubly degenerate with the same parity. In these cases, the interpretation of these SIs may change, which takes case-by-case examination, and the SI expressions are only effective and may become invalid when, for example, the origin point is changed. Thus we fix the coordinate system to avoid these problems by adopting the Bilbao convention [104–107] when calculating SIs. SI formulas are also written in co-irreps following the Bilbao website, where irreps of type-I MSGs are the same as Bilbao and co-irreps of type-III, IV MSGs are generated using a homemade code, with details given in Supplemental Material [90] Sec. M.

To sum up, the SI formulas in generating SIs can be used to express all SIs in other MSGs, except ten corner-case MSGs which have SI formulas given independently using co-irreps in Supplemental Material [90] Sec. H. Here we show an example of MSG 42.222 $Fm'm'2$, which has a $\mathbb{Z}_2$ indicator with expression

$$z_{2,42.222} = N(\bar{\Gamma}_3) - N(\bar{A}_3) \bmod 2, \tag{1}$$

where $N(\bar{K}_i)$ represents the number of co-irrep $\bar{K}_i$. This MSG has MTCI classification $\mathbb{Z}$, the generator of which has weak invariants $\delta_w = (1, 1, 0)$ and all other invariants equal zero. The SI $z_{2,42.222} = 1$ represents this generator as well as all the odd number copies of it. Note that this indicator is different from the choice in Ref. [52].

B. Computation of SIs for topological crystals

In this section, we show how one can calculate the SIs for a given TC. As most of the SIs correspond to some topological invariants, including $z_{2P,i}$, z_{4P}, z'_{2P}, z_{nC}, $z^{\pm}_{nm,0/\pi}$, z_{2,S_4}, and z'_{nC}, their values can be determined directly. For example, the $\mathbb{Z}_2 \times \mathbb{Z}_2 \times \mathbb{Z}_2 \times \mathbb{Z}_4$ indicators defined in $P\bar{1}$ have straightforward meanings:

$$z_{2P,i} = \delta_{w,i} \bmod 2, \quad z_{4P} = 2\delta(P), \tag{2}$$

where $\delta_{w,i} (i = 1, 2, 3)$ is the weak invariant and $\delta(P)$ is the inversion invariant. Note that $z_{4P} = 1, 3$ represent Weyl semimetals [28,36].

However, there also exist many SIs that cannot be read directly from the invariants, including z'_{4P}, z_8, and z_{12}. To determine their value for a TC, we need to find a compatible set of co-irreps for the TC and then calculate the SIs of the co-irrep set. The result does not, however, depend on which particular set we choose as long as it is compatible with the TC. This is because a given set of invariants, that is, a given TC, can only correspond to one possible set of SIs. Therefore, we only need to find one compatible set of co-irreps for the TC and calculate its SI.

Finding compatible co-irreps for an LC is simple, but to a non-LC, TC can be challenging. Fortunately, as shown before that many of the non-LCs in MSGs are adiabatically connected to STIs, the BHZ model describing STIs can be used, which has symmetries of SG 221 plus the TRS, a supergroup to many MSGs. As a result, we can adjust the model parameters such that the BHZ model and the non-LCs share the same set of invariants, and then compute the SIs for the BHZ model, with details in Supplemental Material [90] Sec. L.

The mappings between invariants and SIs only need to be derived for the generating MSGs shown in Table IV. Other MSGs, except the corner cases and Weyl states, either are the supergroups of these generating MSGs or have a different Bravais lattice, and their mappings can be induced from the mappings of the generating MSGs. For corner cases, we derive their mappings case by case in Supplemental Material [90] Sec. H.

C. The mapping from SIs to invariants

So far, we have obtained the mapping from invariants to SIs for topological gapped states protected by all MSGs, listed in Supplemental Material [90] Sec. P. A practically more useful mapping is its inverse, one from SIs to invariants. This is because, on one hand, the SIs only depend on the co-irreps at HSPs, and as such are far easier to obtain in first-principles calculations. On the other hand, the invariants, as shown in the previous section, are directly related to the topological surface states that may be detected experimentally. A mapping from SI to invariants hence links first-principles calculations to experimental observables. These mappings from SIs to invariants are one to many in general, in which a given SI set may be mapped to multiple invariant sets.

Assume an MSG has m linearly independent TCs, which have invariant sets $V_1, V_2, \ldots, V_m$ and SI sets $S_1, S_2, \ldots, S_m$. Given an arbitrary SI set S from the SI group, to find all the possible invariant sets corresponding to it, one needs to solve the linear equation $\sum_{i=1}^{m} x_i S_i = S$, where x_i are coefficients to be determined. The invariant sets corresponding to S can be obtained using the solved x_i. This inhomogeneous linear equation can be solved by first finding a special solution and then adding all the general solutions to its homogeneous counterpart, i.e., the solutions of the corresponding homogeneous linear equation, $\sum_{i=1}^{m} x_i S_i = 0$, which gives the invariant sets that have zero SIs.

Following this line, we have developed an algorithm that automatically computes all possible sets of invariants for a

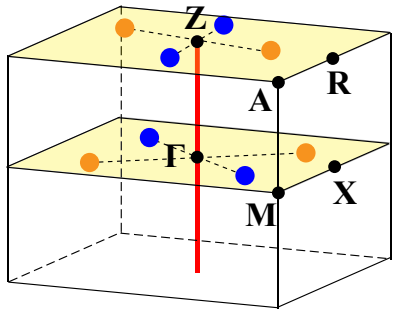

FIG. 5. The Weyl point configuration of MSG 81.37, where the blue and orange dots represent Weyl points of opposite chiralities, the red line represents the S_4 axis, and two yellow planes represent $k_z = 0, \pi$ planes.

given set of SIs. The code and the full results which have been entered into a large table may be downloaded from Ref. [89].

D. Weyl semimetal SIs

Unlike nonmagnetic spinful SGs [30] where for each nonzero SI there exist at least one gapped topological state that corresponds to it, we find many SIs in MSGs can only correspond to gapless Weyl semimetals [52,60,61,70]. As the full mapping from TCs to SIs has been found for each MSG, SI values that do not belong to the image of this mapping necessarily correspond to gapless states. Although these Weyl semimetals have Weyl points at generic momenta or unpinned momenta on a high-symmetry BZ plane, the symmetries of MSGs require their creation or annihilation to happen at HSPs, which makes it possible to detect them using SIs. These Weyl semimetals can be classified into two types, with one being interplane Weyl points that lie between $k_i = 0$ and $k_i = \pi$ planes, and the other being in-plane Weyl points that lie on $k_i = 0$ or π planes, where i denotes the main rotation axis of the MSG. We leave the full discussion of Weyl semimetals to Supplemental Material [90] Sec. I and use one example of type-4 MSG 81.37 $P_C\bar{4}$ to illustrate the basic idea.

MSG 81.37 can host a multiple of four Weyl points on both $k_z = 0/\pi$ planes, with Weyl points connected by S_4 symmetry having opposite chiralities, as shown in Fig. 5. This MSG has MTCI classification $\mathbb{Z}_2$ and SI group $\mathbb{Z}_2 \times \mathbb{Z}_2$. The SI group is larger than the MTCI group. One of the $\mathbb{Z}_2$ indicators can be chosen as z_{2,S_4}, the odd value of which corresponds to the decoration with S_4 invariant $\delta(S_4) = 1$, while the other $\mathbb{Z}_2$ indicator can be chosen as $z_{4C}/2$, the odd value of which represents the Weyl states. Notice that the Weyl points are S_4 symmetric and they can only be annihilated at HSPs on the $k_z = 0/\pi$ plane. Moreover, $z_{4C,k_z=0} = z_{4C,k_z=\pi} = 0$ or 2 always holds (as long as the compatibility relations hold), which means the Weyl points will appear simultaneously on $k_z = 0, \pi$ planes. The in-plane nature of this type of Weyl states is enforced by the $C_2 \cdot T$ symmetry.

IV. DISCUSSION

In this paper, we present a complete topological classification of gapped magnetic crystalline states with significant spin–orbital coupling that can be well-characterized in terms of band structures by explicit construction of real-space TCs, i.e., 3D patterns built by 2D topological patches, including both layer and non-layer constructions. We enumerate all nontrivial topological invariants in MSGs together with their anomalous surface states, and calculate the invariant values for TC generators in each MSG. We also derive the explicit formulas for symmetry indicators in terms of the symmetry representations at high-symmetry momenta. We compute the SI values for each TC generator, and by combining them with the invariant values, we find the complete mappings between SIs and invariants in all MSGs. The SI values not taken by any TCs thus correspond to Weyl semimetals, with possible Weyl point configurations tabulated.

Our diagnosis scheme can be readily applied to the search for realistic magnetic topological materials. For MSGs with nontrivial SI groups, one can extract the co-irrep data from first-principles calculation results [108,109]. When all compatibility relations are satisfied (which means the material is not a HSP or HSL semimetal [57]), the SI values can be obtained by feeding the co-irrep data into the SI formulas. If the SI values indicate a gapped state, by consulting the quantitative mappings between SIs and topological invariants at Ref. [89], one can immediately find the corresponding invariants and furthermore the corresponding surface states. Otherwise, the state is a Weyl semimetal and possible Weyl point configurations can be found in Supplemental Material [90] Sec. I.

For MSGs without SIs but with nontrivial classifications, we list in Supplemental Material [90] Sec. Q the topological invariants for each generator of classification, and one can directly compute the topological invariants to diagnose the states. Although difficult to compute compared to SIs, there are still elaborated tools like Wilson loop formalism [110] to determine various topological invariants such as (mirror) Chern numbers, which may require detailed inspections of the connectivity of the Wilson loop spectrum.

The classification results in this paper, although computed for noninteracting systems, are still meaningful when weak electron-electron interactions are considered. For axion insulators, the $\mathbb{Z}_2$ invariant (i.e., the axion angle θ) is still well-defined in the presence of interactions. The 3D QAH states characterized by nonzero $\mathbb{Z}$ invariants and chiral edge states are also stable against interactions. However, the mirror-protected topological states with mirror Chern numbers $C_m = C_m^+ = -C_m^-$ need to be modified by reducing their invariant C_m from $\mathbb{Z}$ to $\mathbb{Z}_8$ when interactions are involved [111,112].

Given the success of the real-space recipe in previous works [31,32] and the present paper, we are looking forward to its application in other physical systems to obtain the topological classifications, for example, in magnetic electron systems with negligible spin-orbit coupling and TC superconductors, which may involve the reformulations of the building blocks, no-open-edge conditions, and bubble equivalences.

ACKNOWLEDGMENTS

The work was supported by the National Natural Science Foundation (Grants No. 11925408, No. 11921004, and No. 12188101), the Ministry of Science and Technology of China (Grants No. 2018YFA0305700 and No.

2016YFA0302400), the Chinese Academy of Sciences (Grant No. XDB33000000), the K. C. Wong Education Foundation (GJTD-2018-01), and the Informatization Plan of Chinese Academy of Sciences (Grant No. CAS-WX2021SF-0102).

[1] C. J. Bradley and B. L. Davies, Rev. Mod. Phys. **40**, 359 (1968).
[2] T. Moriya and Y. Takahashi, Annu. Rev. Mater. Sci. **14**, 1 (1984).
[3] G. R. Stewart, Rev. Mod. Phys. **56**, 755 (1984).
[4] P. A. Lee, N. Nagaosa, and X.-G. Wen, Rev. Mod. Phys. **78**, 17 (2006).
[5] M. Z. Hasan and C. L. Kane, Rev. Mod. Phys. **82**, 3045 (2010).
[6] X.-L. Qi and S.-C. Zhang, Rev. Mod. Phys. **83**, 1057 (2011).
[7] C.-K. Chiu, J. C. Y. Teo, A. P. Schnyder, and S. Ryu, Rev. Mod. Phys. **88**, 035005 (2016).
[8] N. P. Armitage, E. J. Mele, and A. Vishwanath, Rev. Mod. Phys. **90**, 015001 (2018).
[9] D. J. Thouless, M. Kohmoto, M. P. Nightingale, and M. den Nijs, Phys. Rev. Lett. **49**, 405 (1982).
[10] F. D. M. Haldane, Phys. Rev. Lett. **50**, 1153 (1983).
[11] I. Affleck, T. Kennedy, E. H. Lieb, and H. Tasaki, Phys. Rev. Lett. **59**, 799 (1987).
[12] X.-G. Wen, Int. J. Mod. Phys. B **04**, 239 (1990).
[13] A. Y. Kitaev, Phys. Usp. **44**, 131 (2001).
[14] C. L. Kane and E. J. Mele, Phys. Rev. Lett. **95**, 146802 (2005).
[15] J. E. Moore and L. Balents, Phys. Rev. B **75**, 121306(R) (2007).
[16] L. Fu and C. L. Kane, Phys. Rev. B **76**, 045302 (2007).
[17] A. P. Schnyder, S. Ryu, A. Furusaki, and A. W. W. Ludwig, Phys. Rev. B **78**, 195125 (2008).
[18] A. Kitaev, in AIP Conference Proceedings (American Institute of Physics, College Park, MD, 2009), Vol. 113, pp. 22–30.
[19] S. Ryu, A. P. Schnyder, A. Furusaki, and A. W. Ludwig, New J. Phys. **12**, 065010 (2010).
[20] L. Fu, C. L. Kane, and E. J. Mele, Phys. Rev. Lett. **98**, 106803 (2007).
[21] T. H. Hsieh, H. Lin, J. Liu, W. Duan, A. Bansil, and L. Fu, Nat. Commun. **3**, 982 (2012).
[22] J. C. Y. Teo, L. Fu, and C. L. Kane, Phys. Rev. B **78**, 045426 (2008).
[23] Z. Wang, A. Alexandradinata, R. J. Cava, and B. A. Bernevig, Nature (London) **532**, 189 (2016).
[24] K. Shiozaki and M. Sato, Phys. Rev. B **90**, 165114 (2014).
[25] Z. Song, Z. Fang, and C. Fang, Phys. Rev. Lett. **119**, 246402 (2017).
[26] C. Fang and L. Fu, Sci. Adv. **5**, eaat2374 (2019).
[27] A. M. Turner, Y. Zhang, and A. Vishwanath, Phys. Rev. B **82**, 241102(R) (2010).
[28] T. L. Hughes, E. Prodan, and B. A. Bernevig, Phys. Rev. B **83**, 245132 (2011).
[29] B. J. Wieder, B. Bradlyn, Z. Wang, J. Cano, Y. Kim, H.-S. D. Kim, A. M. Rappe, C. Kane, and B. A. Bernevig, Science **361**, 246 (2018).
[30] Z. Song, T. Zhang, Z. Fang, and C. Fang, Nat. Commun. **9**, 3530 (2018).
[31] Z. Song, S.-J. Huang, Y. Qi, C. Fang, and M. Hermele, Sci. Adv. **5**, eaax2007 (2019).
[32] Z. Song, C. Fang, and Y. Qi, Nat. Commun. **11**, 4197 (2020).
[33] E. Khalaf, H. C. Po, A. Vishwanath, and H. Watanabe, Phys. Rev. X **8**, 031070 (2018).
[34] X.-L. Qi, T. L. Hughes, and S.-C. Zhang, Phys. Rev. B **78**, 195424 (2008).
[35] R. Li, J. Wang, X.-L. Qi, and S.-C. Zhang, Nat. Phys. **6**, 284 (2010).
[36] A. M. Turner, Y. Zhang, R. S. K. Mong, and A. Vishwanath, Phys. Rev. B **85**, 165120 (2012).
[37] C. Yue, Y. Xu, Z. Song, H. Weng, Y.-M. Lu, C. Fang, and X. Dai, Nat. Phys. **15**, 577 (2019).
[38] D. Zhang, M. Shi, T. Zhu, D. Xing, H. Zhang, and J. Wang, Phys. Rev. Lett. **122**, 206401 (2019).
[39] J. Li, Y. Li, S. Du, Z. Wang, B.-L. Gu, S.-C. Zhang, K. He, W. Duan, and Y. Xu, Sci. Adv. **5**, eaaw5685 (2019).
[40] Y. Gong, J. Guo, J. Li, K. Zhu, M. Liao, X. Liu, Q. Zhang, L. Gu, L. Tang, X. Feng *et al.*, Chin. Phys. Lett. **36**, 076801 (2019).
[41] M. M. Otrokov, I. I. Klimovskikh, H. Bentmann, D. Estyunin, A. Zeugner, Z. S. Aliev, S. Gaß, A. Wolter, A. Koroleva, A. M. Shikin *et al.*, Nature (London) **576**, 416 (2019).
[42] E. D. Rienks, S. Wimmer, J. Sánchez-Barriga, O. Caha, P. S. Mandal, J. Růžička, A. Ney, H. Steiner, V. V. Volobuev, H. Groiß *et al.*, Nature (London) **576**, 423 (2019).
[43] R. S. K. Mong, A. M. Essin, and J. E. Moore, Phys. Rev. B **81**, 245209 (2010).
[44] C. Fang, M. J. Gilbert, and B. A. Bernevig, Phys. Rev. B **88**, 085406 (2013).
[45] C.-X. Liu, arXiv:1304.6455.
[46] R.-X. Zhang and C.-X. Liu, Phys. Rev. B **91**, 115317 (2015).
[47] C.-X. Liu, R.-X. Zhang, and B. K. VanLeeuwen, Phys. Rev. B **90**, 085304 (2014).
[48] K. Shiozaki, M. Sato, and K. Gomi, Phys. Rev. B **95**, 235425 (2017).
[49] K. Shiozaki, Progress Theor. Exp. Phys. **2022**, 04A104 (2022).
[50] N. Okuma, M. Sato, and K. Shiozaki, Phys. Rev. B **99**, 085127 (2019).
[51] E. Cornfeld and S. Carmeli, Phys. Rev. Research **3**, 013052 (2021).
[52] L. Elcoro, B. J. Wieder, Z. Song, Y. Xu, B. Bradlyn, and B. A. Bernevig, Nat. Commun. **12**, 5965 (2021).
[53] C. Fang and L. Fu, Phys. Rev. B **91**, 161105(R) (2015).
[54] C. Fang, M. J. Gilbert, and B. A. Bernevig, Phys. Rev. B **86**, 115112 (2012).
[55] H. C. Po, A. Vishwanath, and H. Watanabe, Nat. Commun. **8**, 50 (2017).
[56] B. Bradlyn, L. Elcoro, J. Cano, M. Vergniory, Z. Wang, C. Felser, M. Aroyo, and B. A. Bernevig, Nature (London) **547**, 298 (2017).
[57] T. Zhang, Y. Jiang, Z. Song, H. Huang, Y. He, Z. Fang, H. Weng, and C. Fang, Nature (London) **566**, 475 (2019).
[58] M. Vergniory, L. Elcoro, C. Felser, N. Regnault, B. A. Bernevig, and Z. Wang, Nature (London) **566**, 480 (2019).

[59] F. Tang, H. C. Po, A. Vishwanath, and X. Wan, Nature (London) **566**, 486 (2019).
[60] S. Ono and H. Watanabe, Phys. Rev. B **98**, 115150 (2018).
[61] H. Watanabe, H. C. Po, and A. Vishwanath, Sci. Adv. **4**, eaat8685 (2018).
[62] Y. Xu, L. Elcoro, Z.-D. Song, B. J. Wieder, M. Vergniory, N. Regnault, Y. Chen, C. Felser, and B. A. Bernevig, Nature (London) **586**, 702 (2020).
[63] B. J. Wieder and B. A. Bernevig, arXiv:1810.02373.
[64] J. Ahn and B.-J. Yang, Phys. Rev. B **99**, 235125 (2019).
[65] F. Schindler, A. M. Cook, M. G. Vergniory, Z. Wang, S. S. P. Parkin, B. A. Bernevig, and T. Neupert, Sci. Adv. **4**, eaat0346 (2018).
[66] K. Shiozaki, M. Sato, and K. Gomi, Phys. Rev. B **91**, 155120 (2015).
[67] K. Shiozaki, M. Sato, and K. Gomi, Phys. Rev. B **93**, 195413 (2016).
[68] H. Kim, K. Shiozaki, and S. Murakami, Phys. Rev. B **100**, 165202 (2019).
[69] H. Kim and S. Murakami, Phys. Rev. B **102**, 195202 (2020).
[70] A. Bouhon, G. F. Lange, and R.-J. Slager, Phys. Rev. B **103**, 245127 (2021).
[71] Z. Fang, N. Nagaosa, K. S. Takahashi, A. Asamitsu, R. Mathieu, T. Ogasawara, H. Yamada, M. Kawasaki, Y. Tokura, and K. Terakura, Science **302**, 92 (2003).
[72] X. Wan, A. M. Turner, A. Vishwanath, and S. Y. Savrasov, Phys. Rev. B **83**, 205101 (2011).
[73] G. Xu, H. Weng, Z. Wang, X. Dai, and Z. Fang, Phys. Rev. Lett. **107**, 186806 (2011).
[74] Z. Wang, M. G. Vergniory, S. Kushwaha, M. Hirschberger, E. V. Chulkov, A. Ernst, N. P. Ong, R. J. Cava, and B. A. Bernevig, Phys. Rev. Lett. **117**, 236401 (2016).
[75] J. Kübler and C. Felser, Europhys. Lett. **114**, 47005 (2016).
[76] G. Chang, S.-Y. Xu, H. Zheng, B. Singh, C.-H. Hsu, G. Bian, N. Alidoust, I. Belopolski, D. S. Sanchez, S. Zhang *et al.*, Sci. Rep. **6**, 38839 (2016).
[77] H. Yang, Y. Sun, Y. Zhang, W.-J. Shi, S. S. Parkin, and B. Yan, New J. Phys. **19**, 015008 (2017).
[78] E. Liu, Y. Sun, N. Kumar, L. Muechler, A. Sun, L. Jiao, S.-Y. Yang, D. Liu, A. Liang, Q. Xu *et al.*, Nat. Phys. **14**, 1125 (2018).
[79] Q. Wang, Y. Xu, R. Lou, Z. Liu, M. Li, Y. Huang, D. Shen, H. Weng, S. Wang, and H. Lei, Nat. Commun. **9**, 3681 (2018).
[80] I. Belopolski, K. Manna, D. S. Sanchez, G. Chang, B. Ernst, J. Yin, S. S. Zhang, T. Cochran, N. Shumiya, H. Zheng *et al.*, Science **365**, 1278 (2019).
[81] N. Morali, R. Batabyal, P. K. Nag, E. Liu, Q. Xu, Y. Sun, B. Yan, C. Felser, N. Avraham, and H. Beidenkopf, Science **365**, 1286 (2019).
[82] D. Liu, A. Liang, E. Liu, Q. Xu, Y. Li, C. Chen, D. Pei, W. Shi, S. Mo, P. Dudin *et al.*, Science **365**, 1282 (2019).
[83] S. Nie, G. Xu, F. B. Prinz, and S.-c. Zhang, Proc. Natl. Acad. Sci. **114**, 10596 (2017).
[84] P. Tang, Q. Zhou, G. Xu, and S.-C. Zhang, Nat. Phys. **12**, 1100 (2016).
[85] G. Hua, S. Nie, Z. Song, R. Yu, G. Xu, and K. Yao, Phys. Rev. B **98**, 201116(R) (2018).
[86] K. Kim, J. Seo, E. Lee, K.-T. Ko, B. Kim, B. G. Jang, J. M. Ok, J. Lee, Y. J. Jo, W. Kang *et al.*, Nat. Mater. **17**, 794 (2018).
[87] S. Nie, H. Weng, and F. B. Prinz, Phys. Rev. B **99**, 035125 (2019).
[88] J. Zou, Z. He, and G. Xu, npj Comput. Mater. **5**, 96 (2019).
[89] https://github.com/yjiang-iop/MSG_mapping.
[90] See Supplemental Material at http://link.aps.org/supplemental/10.1103/PhysRevB.105.235138 for background details.
[91] H. Song, S.-J. Huang, L. Fu, and M. Hermele, Phys. Rev. X **7**, 011020 (2017).
[92] S.-J. Huang, H. Song, Y.-P. Huang, and M. Hermele, Phys. Rev. B **96**, 205106 (2017).
[93] R. Thorngren and D. V. Else, Phys. Rev. X **8**, 011040 (2018).
[94] D. V. Else and R. Thorngren, Phys. Rev. B **99**, 115116 (2019).
[95] A. Rasmussen and Y.-M. Lu, Phys. Rev. B **101**, 085137 (2020).
[96] K. Shiozaki, C. Z. Xiong, and K. Gomi, arXiv:1810.00801.
[97] A. Altland and M. R. Zirnbauer, Phys. Rev. B **55**, 1142 (1997).
[98] We remark that obstructed atomic insulators, which may have corner or hinge modes, are not stable topological states and not included in our classification, as their corner or hinge modes can merge into bulk bands without breaking the symmetry or closing the band gap.
[99] B. J. Wieder, K.-S. Lin, and B. Bradlyn, Phys. Rev. Research **2**, 042010(R) (2020).
[100] P. M. Perez-Piskunow and S. Roche, Phys. Rev. Lett. **126**, 167701 (2021).
[101] B. A. Bernevig, T. L. Hughes, and S.-C. Zhang, Science **314**, 1757 (2006).
[102] J. Kruthoff, J. de Boer, J. van Wezel, C. L. Kane, and R.-J. Slager, Phys. Rev. X **7**, 041069 (2017).
[103] Z. Song, T. Zhang, and C. Fang, Phys. Rev. X **8**, 031069 (2018).
[104] M. I. Aroyo, J. M. Perez-Mato, C. Capillas, E. Kroumova, S. Ivantchev, G. Madariaga, A. Kirov, and H. Wondratschek, Z. Kristallogr.—Cryst. Mater. **221**, 15 (2006).
[105] M. I. Aroyo, A. Kirov, C. Capillas, J. Perez-Mato, and H. Wondratschek, Acta Crystallogr. Sect. A: Found. Crystallogr. **62**, 115 (2006).
[106] M. I. Aroyo, J. M. Perez-Mato, D. Orobengoa, E. Tasci, G. de la Flor, and A. Kirov, Bulg. Chem. Commun. **43**, 183 (2011).
[107] L. Elcoro, B. Bradlyn, Z. Wang, M. G. Vergniory, J. Cano, C. Felser, B. A. Bernevig, D. Orobengoa, G. Flor, and M. I. Aroyo, J. Appl. Crystallogr. **50**, 1457 (2017).
[108] Y. He, Y. Jiang, T. Zhang, H. Huang, C. Fang, and Z. Jin, Chin. Phys. B **28**, 087102 (2019).
[109] J. Gao, Q. Wu, C. Persson, and Z. Wang, Comput. Phys. Commun. **261**, 107760 (2021).
[110] N. Varnava, I. Souza, and D. Vanderbilt, Phys. Rev. B **101**, 155130 (2020).
[111] H. Isobe and L. Fu, Phys. Rev. B **92**, 081304(R) (2015).
[112] T. Morimoto, A. Furusaki, and C. Mudry, Phys. Rev. B **92**, 125104 (2015).